This is the accepted manuscript made available via CHORUS. The article has been published as:

Dirac dispersion generates unusually large Nernst effect in Weyl semimetals

Sarah J. Watzman, Timothy M. McCormick, Chandra Shekhar, Shu-Chun Wu, Yan Sun, Arati Prakash, Claudia Felser, Nandini Trivedi, and Joseph P. Heremans

Phys. Rev. B **97**, 161404 — Published 18 April 2018
DOI: 10.1103/PhysRevB.97.161404

Dirac dispersion generates unusually large Nernst effect in Weyl semimetals

Sarah J. Watzman[1], Timothy M. McCormick[2], Chandra Shekhar[3], Shu-Chun Wu[3], Yan Sun[3],
Arati Prakash[2], Claudia Felser[3], Nandini Trivedi[2], Joseph P. Heremans[1,2,4]*

1. Department of Mechanical and Aerospace Engineering, The Ohio State University, Columbus, OH, USA, 43210.
2. Department of Physics, The Ohio State University, Columbus, OH, USA, 43210.
3. Max Planck Institute for Chemical Physics of Solids, Dresden, Germany, 01187.
4. Department of Materials Science and Engineering, The Ohio State University, Columbus, OH, USA, 43210.

Receipt date: XX February 2018

PACS: 72.15.Jf, 72.20.Pa, 72.10.-d

ABSTRACT

Weyl semimetals contain linearly dispersing electronic states, offering interesting features in transport yet to be thoroughly explored thermally. Here we show how the Nernst effect, combining entropy with charge transport, gives a unique signature for the presence of Dirac bands and offers a diagnostic to determine if trivial pockets play a role in this transport. The Nernst thermopower of NbP exceeds its conventional thermopower by a hundredfold, and the temperature dependence of the Nernst effect has a pronounced maximum. The charge neutrality condition dictates that the Fermi level shifts with increasing temperature toward the energy that has the minimum density of states (DOS). In NbP, the agreement of the Nernst and Seebeck data with a model that assumes this minimum DOS resides at the Dirac points is taken as strong experimental evidence that the trivial (non-Dirac) bands play no role in high-temperature transport.

MAIN TEXT

Unique features intrinsic to Weyl semimetals (WSM) lead to interesting galvanomagnetic transport phenomena [1,2]. Preliminary theoretical studies predict that bulk Weyl nodes [3,4] and surface Fermi arcs [5] have magnetothermal and thermomagnetic transport signatures beyond classical semimetal electrical transport signatures. Dirac fermion experimental thermomagnetic data exists [6,7], including magnetic-field-dependent adiabatic Seebeck coefficients [8,9]. While model fits to data exist for PbSnSe [6] and Cd_3As_2[7], here we present a quantitative understanding of the NbP Nernst and Seebeck coefficients without recourse to fitting parameters for temperature or field dependences.

We show that symmetry between the electron-like and hole-like Dirac band portions results in *(i)* a characteristic temperature- and magnetic-field-dependent Nernst thermopower, and *(ii)* a relation between the Nernst and Seebeck coefficients' unique Dirac band signatures. We report and explain the single-crystal NbP isothermal Nernst and magneto-Seebeck effects on samples with large, unsaturated magnetoresistances and ultrahigh mobilities. In the zero-temperature limit the NbP band structure has 24 Weyl points and several trivial pockets [2]. Here we show that with increasing temperatures, electrons/holes in the NbP symmetric Dirac bands dominate transport as electrochemical potential $\mu(T)$ moves toward the Dirac point, minimizing contributions from the trivial bands (i.e., no Dirac dispersion near the electrochemical potential).

The Nernst effect is a decreasing function of temperature in classical, non-Dirac semimetals like Bi [10], except in the phonon-drag regime, excluded here [9]. In NbP, the Nernst effect temperature dependence is non-monotonic with a maximum at T_M. The experimental Nernst thermopower is two orders of magnitude larger than the Seebeck coefficient. We show these two effects as specific to Dirac bands. When electrons and holes coexist in equal density in symmetric bands, the Seebeck coefficient tends to zero and the Nernst effect (the sum of the electron and hole contributions [11]) is large. Furthermore, the local charge-neutrality condition in undoped semiconductors and semimetals dictates that $\mu(T)$ is located at the energy where the density of states (DOS) is minimal. When defects or aliovalent impurities add an extrinsic charge-carrier density, $\mu(T)$, in the limit $T \rightarrow 0$K, falls in a band at μ_0. As the temperature increases such that thermally-induced intrinsic charge carriers outnumber extrinsic carriers, $\mu(T)$ tends toward the energy minimizing DOS. We demonstrate that in NbP, this energy is the Dirac point of the carriers in the W2 band identified in Ref [2], which we define as the energy scale zero. This claim is based on a model using independently derived values for the parameter μ_0 and the carrier scattering time τ; applying no fitting parameters. In this model, the Nernst coefficient first increases with increasing temperature for $T<T_M$ as $\mu(T)$ starts from μ_0 and tends toward the Dirac point, thereby increasing compensation between electrons and holes. For $T>T_M$, the Nernst coefficient decreases as the Fermi distribution broadens with increasing temperature and the relative contribution of non-linear band dispersions increases. Simultaneously, the Seebeck coefficient for $T>T_M$ tends to zero due to compensation in the dispersion. This model tracks experiments quantitatively and qualitatively, providing strong evidence that Dirac bands dominate conduction and $\mu(T)$ reaches the Dirac point at $T=T_M$. We conclude that the trivial bands contribute little to transport at high temperature ($T>T_M$) in NbP. Similar temperature dependences are observed in experimental Nernst coefficients of other Weyl semimetals, indicating similar behavior, although this must be investigated individually.

The maximum Nernst thermopower found, α_{xyz}(9T, 109K)~800 μV/K, is remarkable, surpassing traditional thermoelectric semiconductors' thermopower (~200–300 μV/K). Developing materials where this happens near room temperature would be technologically significant because output from a transverse Nernst thermoelectric generator or Ettingshausen cooler scales intrinsically with device size [12,13], does not require separate n- and p-type legs, and functions over large temperature differences without staging or cascading, offering advantages over conventional thermoelectric modules.

With magnetic-field application along the z-axis <001> and temperature gradient perpendicular along the x-axis, the isothermal Nernst thermopower α_{xyz} is the transverse electric field measured along the y-axis. The isothermal Seebeck coefficient α_{xxz} measures longitudinal electric field along the x-axis:

$$\alpha_{xyz} \equiv \left. {E_y(H_z)}\middle/{-\nabla_x T} \right|_{\nabla_y T=0} ;\ \alpha_{xxz} \equiv \left. {E_x(H_z)}\middle/{-\nabla_x T} \right|_{\nabla_y T=0} \qquad (1)$$

The Nernst coefficient is defined as $N_{xyz} \equiv \left. {d\alpha_{xyz}}\middle/{dH_z} \right|_{\nabla_y T=0,H_z}$. Unlike prior work [9], we study these quantities *isothermally*, such that $\nabla_y T=0$ [14]. The distinction between isothermal and adiabatic thermomagnetic transport is fundamental [14] and detailed in the supplement [15]; transport theory models isothermal coefficients, not adiabatic ones.

Previous two-band Drude models fit electrical transport in compensated semimetals well, e.g., $Pb_{1-x}Sn_xSe$ [6] and WTe_2 [16]. Nevertheless, we present a WSM Hamiltonian-based theory [17], which does not invoke each band contribution in a multiband system, but instead, an integral covering energies lower and higher than that of the Dirac point. Fig. 1(a) plots the energy band structure. Fig. 1(b) gives a two-dimensional picture of one Dirac band. The model is solved selfconsistently for $\mu(T)$, which moves to the nodal energy with increasing temperature on a scale of $T/\mu_0/k_B$, Fig. 1(c). This hypothesized $\mu(T)$ behavior ignores any trivial band contribution and is crucial to the temperature-dependent Nernst effect. The supplement [15] provides thermomagnetic tensor-element calculations from the WSM Hamiltonian in the Boltzmann formalism, and calculates the isothermal Seebeck and Nernst coefficients as a function of magnetic field and temperature. The linear Dirac band dispersion results in a quadratic dependence of the DOS's energy dependence. If the relaxation time also has an energy dependence that is a power law of energy, $\tau(\varepsilon)=\tau_0\varepsilon^{\lambda}$ with λ an integer, the Fermi functions entering the integrals at zero magnetic field have analytical solutions, obviating the need for the Bethe-Sommerfeld expansion [18], valid only in the degenerate limit. Therefore, analytic solutions can be derived for the thermopower and the low-field Nernst coefficient of symmetric Dirac bands, valid at all temperatures. For λ=0 (energy-independent relaxation time), they are:

$$\begin{aligned}
\left|\alpha_{xxz}\right| &= \frac{2\pi^2}{3}\frac{k_B}{e}\frac{\mu}{k_B T}\left[\left(\frac{k_B T}{\mu}\right)^2 \Big/ 1+\frac{\pi^2}{3}\left(\frac{k_B T}{\mu}\right)^2\right] \\
\lim_{H_z\to 0} N_{xyz} &= \frac{\pi^2}{3}\frac{\tau v_F^2}{T}\left[\left(\frac{k_B T}{\mu}\right)^2 \Big/ 1+\frac{\pi^2}{3}\left(\frac{k_B T}{\mu}\right)^2\right]
\end{aligned} \qquad (2).$$

These functions quantitatively describe most of the important features of the low-field Nernst and Seebeck coefficients including the non-monotonicity of the temperature dependence. They predict that the low-field Nernst coefficient will maximize at $T_{ML} \simeq \sqrt{3}/\pi\ \mu_0/k_B$, above which it will decrease following a $1/T$ law. The Nernst coefficient high-field slope must be derived from numerical calculations in the supplement [15] and will have a maximum at $T_{ML} \simeq \mu_0/k_B$. Theory still requires that two parameters, μ_0 and τ, be quantitative. Comparing theory and experiment, these will be derived independently from the experimental Nernst and Seebeck coefficients: μ_0 from de Haas-van Alphen (DHVA) and Shubnikov-de Haas (SDH) oscillations, and τ from resistivity.

This work experimentally characterizes a 2.25 x 1.29 x 0.52 mm single crystal of NbP, made following Ref. [2] and fully characterized with resistivity, thermal conductivity, specific heat, and magnetization (see supplement [15]), confirming the crystal had properties similar to that in Ref [2]. The sample was mounted on a silicon backing plate with a temperature gradient applied along x and magnetic field along z <001>. Measurements follow the conventions of Eq. 1 with (x,y,z) coordinates orthonormal (x and y orientations lie unidentified in the <001> plane). The silicon plate underlying the sample thermally short-circuits it so that the temperature gradient established in the silicon also is imposed on the NbP with $\nabla_y T \approx 0$, which is an isothermal mount. This is mounted in the Thermal Transport Option on a Quantum Design Physical Property Measurement System modified for isothermal Nernst and Seebeck measurements. This mount differs from the manufacturer-recommended conventional adiabatic mount used in Ref. [9]. The supplement [15] shows theoretically and experimentally the difference between isothermal and adiabatic measurements. For emphasis, this difference cannot be eliminated by data post-processing, such as by symmetrizing even and odd in-field parts.

The experimental Nernst effect results are shown in Figs. 2(a) (magnetic field dependence of Nernst thermopower) and 3(a) (temperature dependence of Nernst coefficient). α_{xyz} is an odd function of H_z with a higher slope near zero magnetic field than at high field. We see a large, unsaturated Nernst thermopower with a maximum exceeding 800 μV/K at 9T, 109K. The Nernst coefficient temperature dependence taken at low field ($|H_z|$<2T) and at high field (3T<$|H_z|$<9T) are non-monotonic, with a maximum around T_{ML}~55±10K for low-field and T_{MH}~90±10K for high-field, consistent with the model prediction $T_{ML} \simeq \sqrt{3}/\pi \, T_{MH}$. The Fig. 3(a) inset shows the Seebeck coefficient α_{xxz} temperature dependence; α_{xxz} is nearly two orders of magnitude smaller than the maximum 9T Nernst thermopower, and its absolute value is much smaller than the high-field Nernst effect at all temperatures. The α_{xxz} temperature dependence has a broad minimum around $T_{MS} \approx$ 60-100K. No $\alpha_{xxz}(H_z)$ magnetic-field dependence is observed within instrument sensitivity. This result does not contradict prior measurements [9] of the adiabatic magneto-Seebeck coefficient; those reflect an α_{xyz} contribution due to a finite $\nabla_y T$ induced by a thermal Hall effect resulting from the adiabatic measurement technique (see supplement [15]).

To compare theory to experiment quantitatively, we determine first the Fermi level value, μ_0, setting the temperature scale. At low temperatures (Fig. 2(a) inset), the Nernst thermopower exhibits SDH oscillations. The periods observed in SDH and DHVA oscillations in the magnetization (see supplement [15]) correspond well within our measurement error bars to those of Ref. [19]. These periods are used in conjunction with density functional theory (DFT) to derive μ_0's position vis-à-vis the Weyl points in the 0K limit. DFT calculations were performed using the

Vienna *ab-initio* Simulation Package [20] with a generalized gradient approximation [21]. The tight-binding model Hamiltonian was calculated by projecting Bloch states onto maximally localized Wannier functions [22] used for generating Fermi surfaces. In the 0K limit, there are two Weyl-point types in NbP: one in the k_z=0 plane and the other around the k_z= π/c plane along <001>. The latter type contributes to transport [23,24]. We calculated the quantum oscillation periods for both electron and hole pockets with the magnetic field applied both parallel and perpendicular to <001> as a function of the hypothetical position of μ_0. The DFT calculation accuracy is limited to several meV, making a perfect fit of all experimental oscillation frequencies with all calculations unrealistic. A μ_0=-8.2±0.7 meV value range satisfies most of the observed oscillations (Fig. 4) and sets μ_0 in the valence band, consistent with the positive thermopower observed at T<25K. The specific heat of the sample is analyzed (see supplement, Eq. S5 [15]) in terms of a linear electronic and a phonon term; the linear term has a coefficient γ=1.5 10^{-4} J/mol-K^2, comparing well with the calculated γ=1.45 10^{-4} J/mol-K^2 derived from the DOS at μ_0=-8.2 meV.

The second parameter needed for quantitative comparison is scattering time τ, assumed to be energy and temperature independent. DFT-derived values of v_F~2x10^5 m s^{-1} (confirmed by ARPES) and measured resistivity (see supplement [15]) yield τ~10^{-13} s.

The model (see supplement, Eq. S11 [15]) now can be compared to experimental data with all parameters determined independently of the Nernst and Seebeck measurements themselves. The calculated field and temperature dependences are reported in Figs. 2(b) and 3(b), showing exceptional agreement to experimental results, apart from the sign change theory predicts for the low-field Nernst effect below 40K. The amplitudes agree within a factor of 4, remarkable given the uncertainty of τ. Fig. 3 shows in theory and experiment that the high-field Nernst coefficient peaks at $T_{MH} \simeq \mu_0/k_B$, whereas near zero field, the Nernst coefficient peaks at $T_{ML} \simeq \sqrt{3}/\pi \; \mu_0/k_B$. The maximum at $T_{MS} \simeq T_{ML}$, calculated for the Seebeck coefficient absolute value (Eq. 2), also is observed.

The model ignores trivial pockets in the Fermi surface by hypothesis, whereas band structure calculations valid in the 0K limit show they exist. When they are included in the Nernst and Seebeck effect calculations, the model diverges from experiment (see supplement [15]). We propose this as experimental evidence that non-Dirac bands do not contribute significantly to transport at temperatures above μ_0/k_B. The behavior of α_{xxz} (Fig. 3(a) inset) strengthens this argument. α_{xxz} tends to zero, a value reached rigorously in a Dirac band when $\mu(T)=0$ (Eq. 2). If trivial pockets contributed to thermopower, $\alpha_{xxz}(T)$ would become metallic and increase monotonically with increasing temperature, as for Bi [10]. The partial thermopowers for the different trivial pockets of the Fermi surface that exist at low temperature can be inferred from the low temperature Fermi energies calculated for these pockets (see supplement [15]). If these pockets had been present at room temperatures, their partial thermopowers would have been of the order of 50-500 μV/K, compared to which the experimental value in Fig. 3a is factually zero. Because an accidental cancellation over a wide temperature range of the contributions of all non-Dirac bands is highly unlikely, we offer this as a *reductio ad absurdum* proof that the trivial pockets do not contribute. Furthermore, the near-perfect compensation between electron and hole pockets in the Dirac bands also explains the galvanomagnetic properties [2]. Although our analysis cannot identify the reason for this observation, the band structure temperature dependence might be responsible for this: most semiconductor band gaps increase (PbTe) or decrease (GaAs) by ~100 meV from cryogenic to room temperatures. Given the energy scale for Dirac fermions relevant to transport is an order of magnitude less, this may cause the disappearing trivial pocket importance with increasing temperature.

In conclusion, we experimentally and theoretically explored thermomagnetic transport in the inversion-symmetry-breaking WSM NbP. Two regimes in Nernst thermopower are seen: one for $H_z>|3T|$, and the other $H_z<|2T|$; both have non-monotonic temperature dependences. The theory explaining these properties quantitatively shows them to be Dirac band transport signatures, with no measureable contributions from trivial pockets above ~100K. Theory and experiment show that as the chemical potential shifts to the Dirac point energy with increasing temperature, the Nernst effect is maximized. At temperatures above the peak temperature, the Fermi function derivative broadens, leading states away from the Weyl nodes to contribute more to transport, lowering the Nernst thermopower and coefficient. The Nernst thermopower α_{xyz}(9T, 109K) exceeds 800 μV/K, surpassing the Seebeck thermopower α_{xxz} by two orders of magnitude. This study offers an understanding of the temperature dependence of the electrochemical potential position vis-à-vis the Weyl point and shows a direct connection between the Nernst effect and topology, a potentially robust mechanism for investigating topological states and the chiral anomaly.

We acknowledge the following support: SJW is supported by the U. S. National Science Foundation Graduate Research Fellowship Program under grant number DGE-0822215. TMM, AP, and JPH are supported by the Center for Emergent Materials, an NSF MRSEC, under grant number DMR-1420451. JPH is also supported by the U. S. Army Research Office MURI under grant number W911NF-14-0016. NT is supported by funding from NSF-DMR-1309461.

FIGURE LABELS

Fig. 1: Electrochemical potential band structure and motion with temperature. (a) Two-dimensional electronic dispersion relation (Eq. S6 in the supplement [15]) used in modeling NbP transport properties. (b) Two-dimensional dispersion around a single Dirac cone where, at low temperatures, the electrochemical potential lies in the valence band at an energy μ_0 below the Dirac point. (c) Calculated $\mu(T)$ temperature dependence shows it moving towards the Weyl node energy with increasing temperature, from $|\mu_0|$, whether in the conduction or valence band. The energy scale is set to unity at $|\mu_0|$, and the temperature scale to unity at $|\mu_0/k_B|$.

Fig. 2: Nernst thermopower, α_{xyz} magnetic field dependence. (a) Measured Nernst thermopower as a function of applied magnetic field at various temperatures. The sharper slope for $|H|$ below ~2T is the low-field regime; above ~3T is the high-field regime. Systematic geometric error on the Nernst thermopower field dependence is ~17%. Data are not symmetrized. Inset shows the Nernst voltage magnetic field dependence measured at 4.92K in a 2.17 mK temperature gradient. SDH oscillations are visible and correspond to DHVA periods measured in the magnetization. (b) Calculated at select temperatures, Nernst thermopower magnetic-field dependence given in SI and natural units that correspond well experimentally. The magnetic field is the product of the in-plane lattice constant a and magnetic length $L_B \equiv \sqrt{\hbar c / eB}$; thermopower is k_B/e, and temperature in given units of $|\mu_0/k_B|$.

Fig. 3: Nernst coefficient, N_{xyz} temperature dependence. (a) Measured Nernst coefficient plotted as a function of temperature (low-field regime in red, high-field in blue). The Nernst coefficient peaks near 50K (low-field) and 90K (high-field). Inset shows conventional thermopower temperature dependence, with a maximum near 8 µV/K, over two orders of magnitude smaller than the maximum Nernst thermopower. No magneto-thermopower is observed when a 9T magnetic field is applied parallel to the <001> axis. Error bars represent a 95% confidence interval on the systematic error standard deviation, excluding geometric error on the sample mount. (b) Calculated temperature dependence of the Nernst coefficient in the low-field (red) and high-field (blue) regimes. The given SI and natural units correspond very well without fitting

Fig. 4: Electrochemical potential at 0K from DHVA periods and DFT calculations. Calculated (data points) and experimental (horizontal lines) values of the DHVA oscillation periods are

shown as a function of μ_0 in the 0K limit, as measured from the W2 Dirac point . The μ_0=-8.2±0.7 meV values are represented by the hatched region, with the best overall fit in that box.

---

[1] X.-P. Huang, F. Anderegg, E. M. Hollmann, C. F. Driscoll, and T.M. O'Neil, *Phys. Rev. Lett.* **5**, 31023 (2015).

[2] C. Shekhar, A. K., Nayak, Y. Sun, M. Schmidt, M. Nicklas, I. Leermakers, U. Zeitler, Y. Skourski, J. Wosnitza, Z. Liu, Y. Chen, W. Schnelle, H. Borrmann, Y. Grin, C. Felser, and B. Yan, *Nat. Phys*. **11**, 645-649 (2015).

[3] R. Lundgren, P. Laurell, and G. A. Fiete, *Phys. Rev. B* **90**, 165115 (2014).

[4] G. Sharma, P. Goswami, and S. Tewari, *Phys. Rev. B* **93**, 035116 (2016).

[5] T. M. McCormick, S. J. Watzman, J. P. Heremans, and N. Trivedi, *arXiv: 1703.04606* (2017).

[6] T. Liang, Q. Gibson, J. Xiong, M. Hirschberger, S. P. Koduvayur, R. J. Cava, and N. P. Ong, *Nat. Commun* **4**, 2696 (2013).

[7] T. Liang, J. Lin, Q. Gibson, T. Gao, M. Hirschberger, M. Liu, R. J. Cava and N. P. Ong, *Phys. Rev. Lett.* **118**, 136601 (2017).

[8] M. Hirschberger, S. Kushwaha, Z. Wang, Q. Gibson, S. Liang, C. A. Belvin, B. A. Bernevig, R. J. Cava, and N. P. Ong, *Nat. Mater.* **15**, 1161-1165 (2016).

[9] U. Stockert, R. D. dos Reis, M. O. Ajeesh, S. J. Watzman, M. Schmidt, C. Shekhar, J. P. Heremans, C. Felser, M. Baenitz, and M. Nicklas, *J. Phys. Cond. Mat.* **29**, 325701 (2017).

[10] I. Ya. Korenblit, M. E. Kusnetsov, and S. S. Shalyt, *Zh. Eksp. Teor. Fiz.* **56** 8-20 (1969) [Translated from Russian, *Sov. Phys. JETP* **29**, 4-10 (1969)].

[11] E. H. Putley, *The Hall Effect and Related Phenomena*, Butterworths, London (1960).

[12] H. J. Goldsmid, *Introduction to thermoelectricity*, Springer Verlag, Berlin (2010).

[13] S. R. Boona, R. C. Myers, and J. P. Heremans, *Energy Environ. Sci*. **7**, 885-910 (2014).

[14] T. C. Harman and J. M. Honig, *Thermelectric and Thermomagnetic Effects and Applications*, McGraw-Hill, New York (1967).

[15] See Supplemental Material at [URL will be inserted by publisher]. The supplemental materials contain a description of the difference between adiabatic and isothermal thermomagnetic measurements; further sample characterization data (electrical conductivity, magnetoresistance and Hall effect, thermal conductivity, specific heat, and magnetization data); the derivation of the low-temperature electrochemical potential from de Haas-van Alphen oscillations; the process followed to obtain temperature and field dependence of the analytic thermopower and low-field

---

Nernst coefficient; a theoretical analysis of effects of multiple Weyl nodes and trivial pockets; and plots of the analytical formulae in the main text.

[16] Z. Zhu, X. Lin, J. Liu, B. Fauqué, Q. Tao, C. Yang, Y. Shi, and K. Behnia, *Phys. Rev. Lett*. **114**, 176601 (2015).

[17] T. M. McCormick, I. Kimchi, and N. Trivedi, *Phys. Rev. B* **95**, 075133 (2017).

[18] A. Sommerfeld and H. Bethe, *Elektronentheorie de Metalle*, Handbuch der Physik 24/2 333-622, Springer Verlag, Berlin (1939).

[19] J. Klotz, S.-C. Wu, C. Shekhar, Y. Sun, M. Schmidt, M. Nicklas, M. Baenitz, M. Uhlarz, J. Wosnitza, C. Felser, and B. Yan, *Phys. Rev. B* **93**, 121105(R) (2016).

[20] G. Kresse and J. Furthmüller, *Comput. Mater. Sci.* **6**, 15-50 (1996).

[21] J. P. Perdew, K. Burke, and M. Ernzerhof, *Phys. Rev. Lett.* **77**, 3865 (1996) (Erratum *Phys. Rev. Lett.* **78**, 1396 (1997)).

[22] N. Marzari and D. Vanderbilt, *Phys. Rev. B* **56**, 12847 (1997).

[23] H. Weng, C. Fang, Z. Fang, B. A. Bernevig, and X. Dai, *Phys. Rev. X* **5**, 011029 (2015).

[24] S.-M. Huang, S.-Y. Xu, I. Belopolski, C.-C. Lee, G. Chang, B. Wang, N. Alidoust, G. Bian, M. Neupane, C. Zhang, S. Jia, A. Bansil, H. Lin, and M. Z. Hasan, *Nat. Comm*. **6**, 7373 (2015).

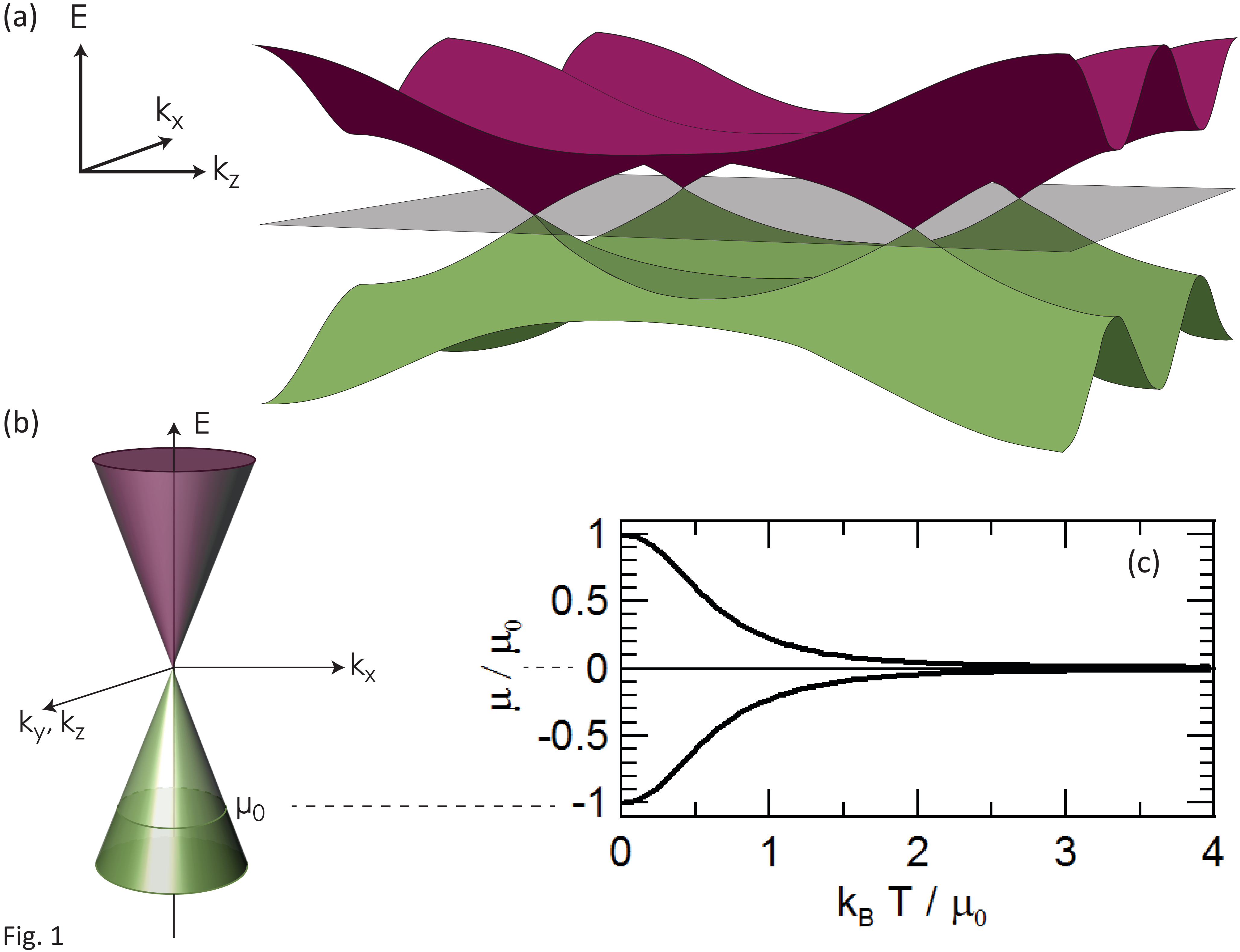

Fig. 1

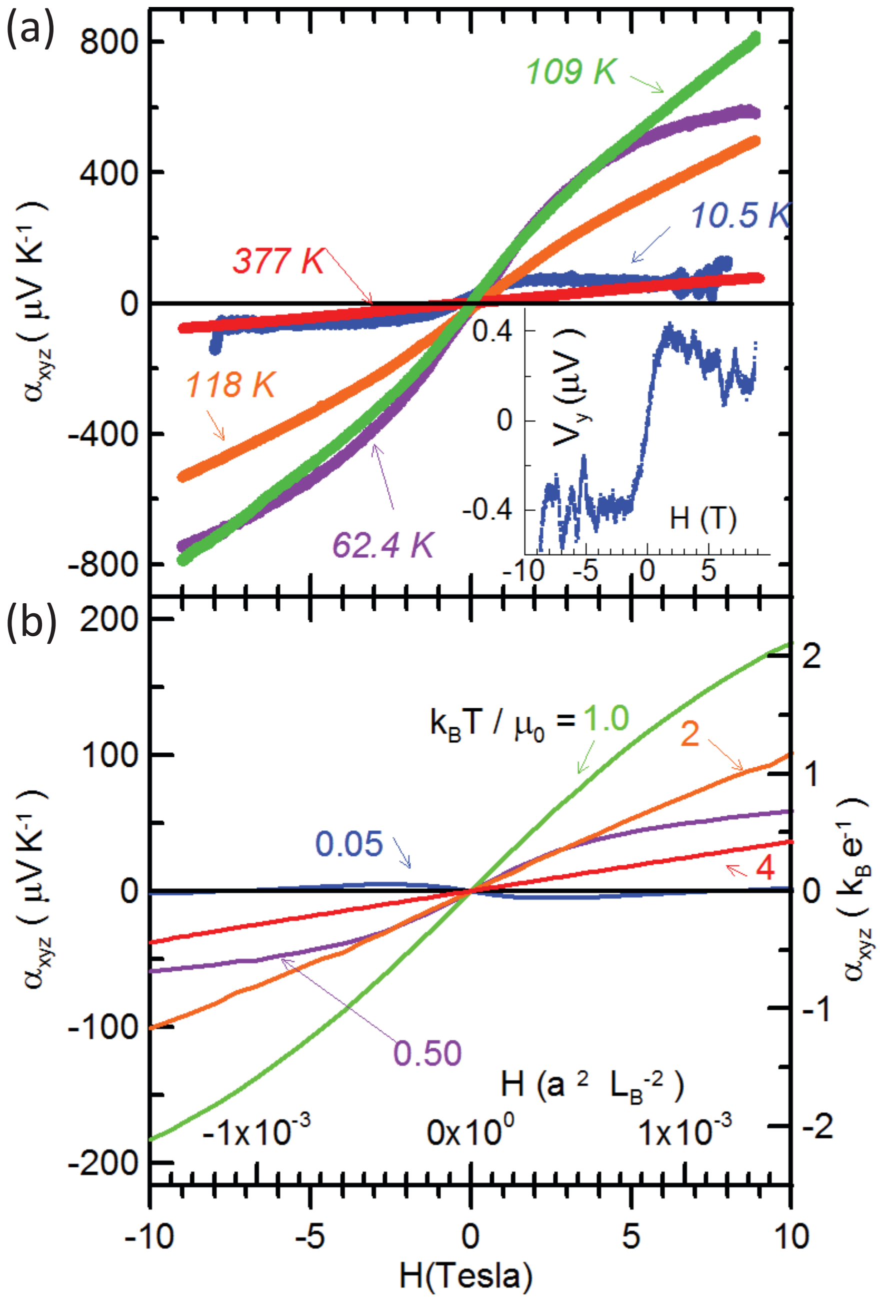
(a)
800
400
0
-400
-800
α_{xyz} (μV K^{-1})
109 K
10.5 K
377 K
118 K
62.4 K
0.4
0
-0.4
V_y (μV)
H (T)
-10
-5
0
5
(b)
200
100
0
-100
-200
α_{xyz} (μV K^{-1})
k_BT / μ_0 = 1.0
2
0.05
4
0.50
H (a ^{2} L$_B^{-2}$)
-1x10^{-3}
0x10^0
1x10^{-3}
2
1
0
-1
-2
α_{xyz} (k$_B$ e^{-1})
-10
-5
0
5
10
H(Tesla)

Fig. 2

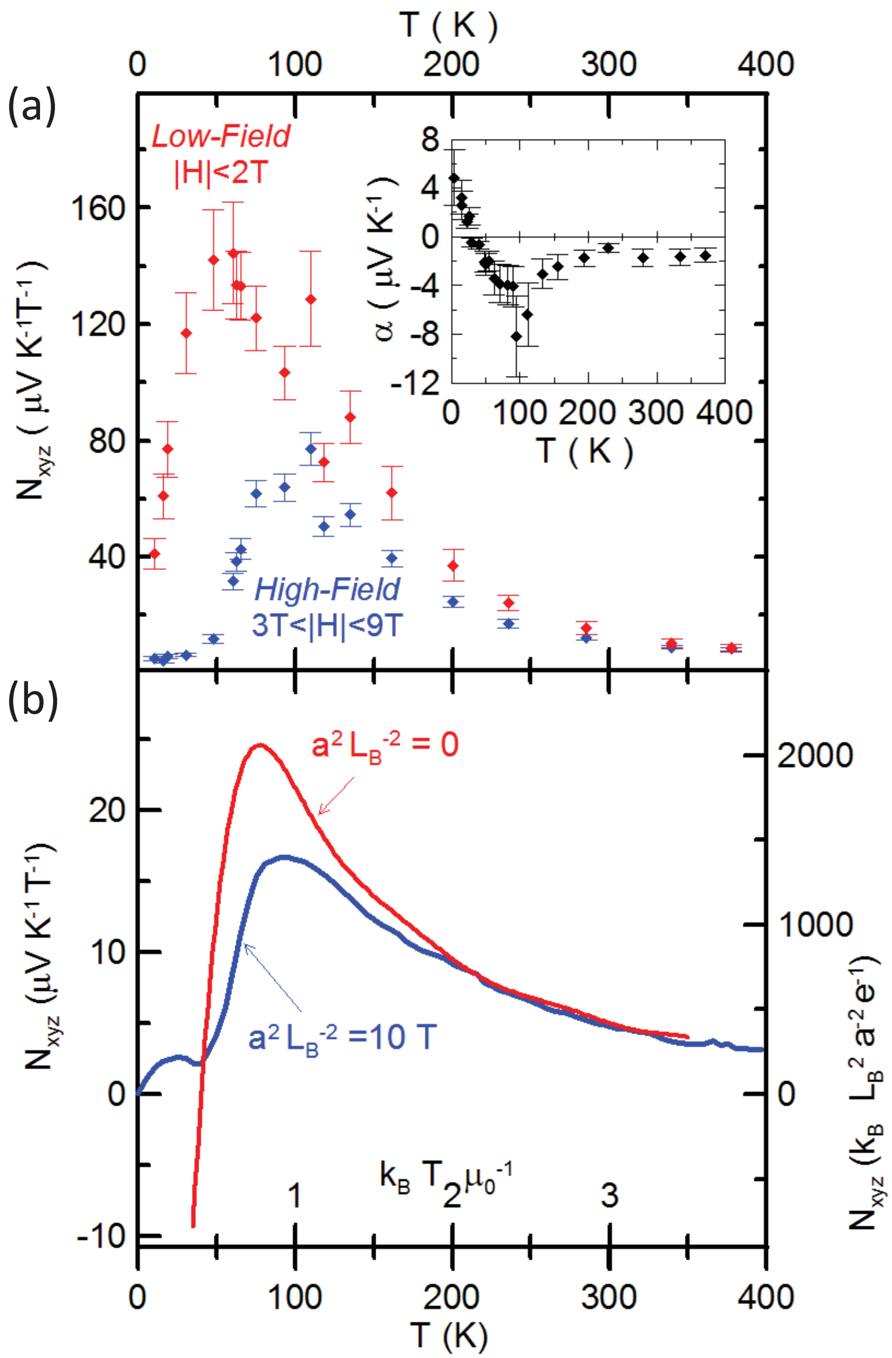
T (K)
0
100
200
300
400
(a)
Low-Field
|H|<2T
N$_{xyz}$ (μV K^{-1}T^{-1})
160
120
80
40
High-Field
3T<|H|<9T
α (μV K^{-1})
8
4
0
-4
-8
-12
0
100
200
300
400
T (K)
(b)
a^2 L$_B$$^{-2}$ = 0
a^2 L$_B$$^{-2}$ =10 T
N$_{xyz}$ (μV K^{-1} T^{-1})
20
10
0
-10
2000
1000
0
N$_{xyz}$ (k$_B$ L$_B$^{2} a^{-2} e^{-1})
k$_B$ T$_2$μ$_0$$^{-1}$
1
3
0
100
200
300
400
T (K)

Fig. 3

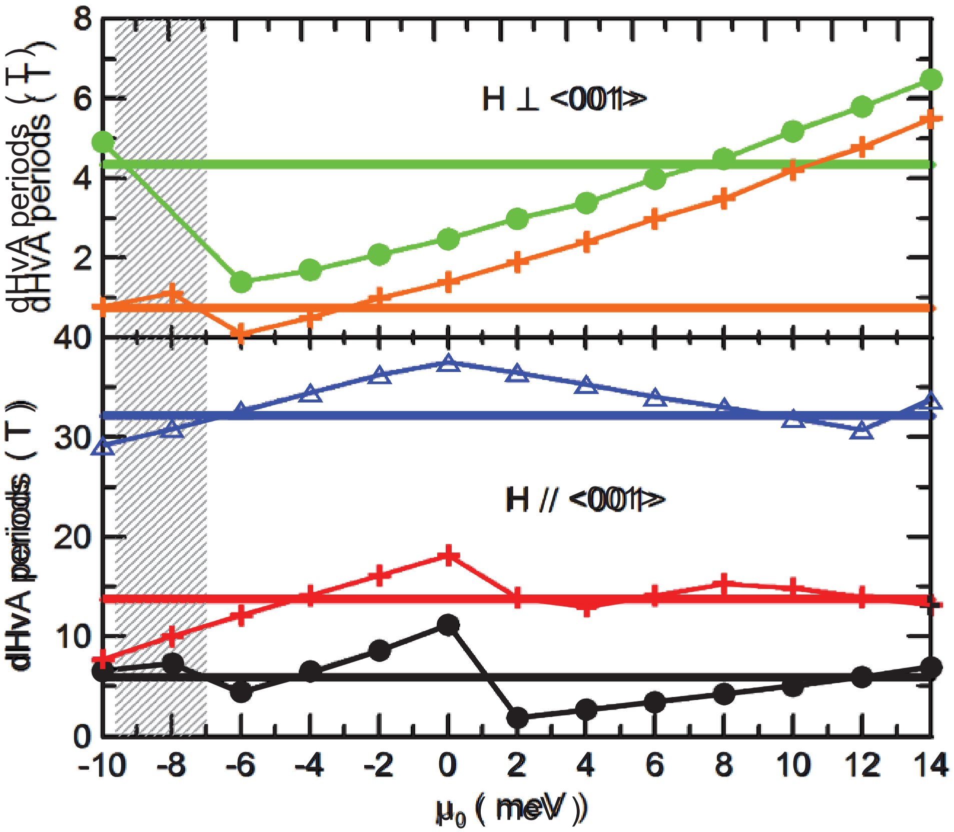
dHvA periods (T)
H ⊥ <001>
H // <001>
8
6
4
2
40
30
20
10
0
-10
-8
-6
-4
-2
0
2
4
6
8
10
12
14
μ0 (meV)